Experimental and theoretical study of pattern identification in physical systems with O(2) symmetry

by

Rory Hartong-Redden

A dissertation submitted in partial satisfaction of the
requirements for the degree of
Bachelor of Science

in

Physics

of the
UNIVERSITY OF CALIFORNIA, SANTA BARBARA

Committee in charge:
Professor Rouslan Krechetnikov, Chair
Professor Deborah Fygenson
Professor Jeff Moehlis

Summer 2010

The dissertation of Rory Hartong-Redden is approved:

Chair Date

Date

Date

University of California, Santa Barbara

Summer 2010

Experimental and theoretical study of pattern identification

in physical systems with O(2) symmetry

by

Rory Hartong-Redden

Abstract

Experimental and theoretical study of pattern identification

in physical systems with O(2) symmetry

by

Rory Hartong-Redden

Bachelor of Science in Physics

University of California, Santa Barbara

Professor Rouslan Krechetnikov, Chair

In this thesis we study pattern identification in systems with O(2) symmetry, e.g. on a circular domain. The study is motivated by a recent discovery of systems in the context of fluid dynamics where instabilities of different wavenumbers may co-exist and thus lead to several single-wavenumber patterns superimposed with a random phase-shift between them. A new experimental setup using stereo high-speed cameras enables a quantitative description of these patterns. Identification of such patterns from experimental data is complicated by the lack of a theoretical basis and by the presence of experimental uncertainties and possible missing points in the data. We present both a theoretical framework and an example of application – the crown structure analysis in the drop splash problem.

Professor Rouslan Krechetnikov
Dissertation Committee Chair

Contents

List of Figures

Acknowledgments

I would like to thank my advisor, Professor Rouslan Krechetnikov, who has consistently held me to a high standard and patiently guided my research. I would also like to thank the other members of my committee: Professors Deborah Fygenson and Jeff Moehlis for their support.

Chapter 1

Introduction

1.1 Motivation

The photo of the milk crown by Edgerton, figure 1.1(c), has fascinated the public and scientists alike for decades. A key question is why there are exactly 24 spikes in the photo. Until the formation of the crown with spikes the system has cylindrical symmetry, i.e. the system (film and droplet) looks the same if you rotate about the axis of the falling droplet. This fact implies that an instability mechanism is responsible for generating the crown which breaks the symmetry. Krechetnikov and Homsy proposed a Richtmayer-Meshkov type instability mechanism [11], while others have proposed Rayleigh-Taylor and Rayleigh-Plateau [7, 5] types. A consensus has not yet been reached in part due to a lack of quantitative analysis of the patterns present in the various drop splash crowns.

Analyzing along-the-edge instability of the liquid sheet [9, 10] shown in figure 1.2(a) it was found that the linear evolution of the Fourier coefficient f_{kn}, $k \in \mathbb{R}$ and $n \in \mathbb{N}$, of the interfacial

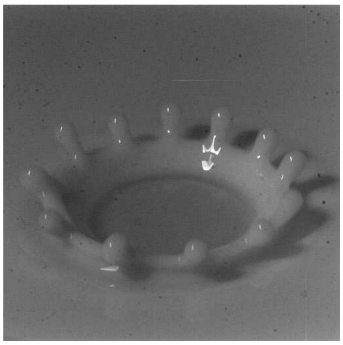

(a) A recent image of a regular pattern.

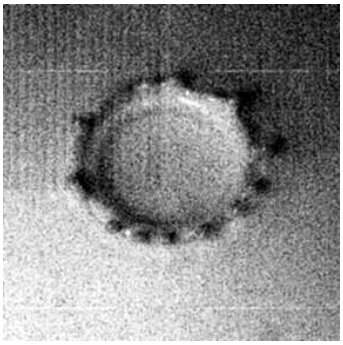

(b) A recent image of an irregular or “frustrated” pattern [11].

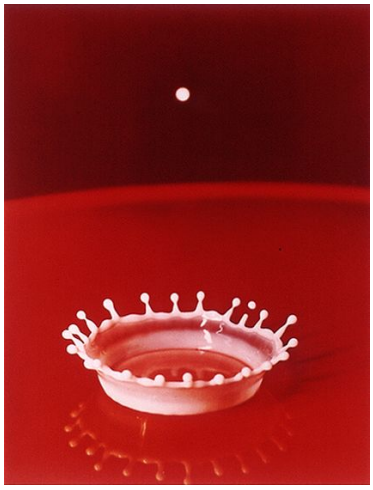

(c) The milk coronet photographed by Edgerton in 1957 [6].

Figure 1.1: Different crowns resulting from impact of a milk droplet on a wetted surface.

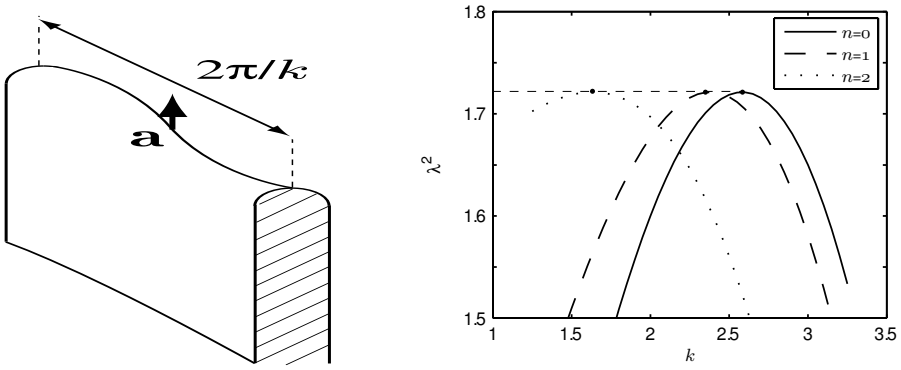

(a) along-the-edge instability; k is the wavenumber and **a** is the acceleration.

(b) Growth rate; $Bo = 20$ and $g = 1$.

Figure 1.2: Growth rates and wavenumber selection.

perturbation f' obeys

$$\frac{\mathrm{d}^2 f_{kn}}{\mathrm{d}t^2} + \sqrt{n^2+k^2}\left\{Bo^{-1}(n^2+k^2) - g\right\} f_{kn} = 0, \tag{1.1}$$

where Bo is the Bond number. The corresponding dispersion relation

$$\lambda^2 = -\sqrt{n^2+k^2}\left\{Bo^{-1}(n^2+k^2) + g\right\}, \tag{1.2}$$

suggests that the growth rate λ depends only on the modulus of the two-dimensional wavenumber $(k^2+n^2)^{1/2}$. The maximum growth rate is achieved at

$$\lambda^* = \max \lambda = \lambda|_{k^* = \sqrt{-\frac{g}{3}Bo - n^2}} = \left[\frac{4}{27} Bo\,(-g)^3\right]^{1/4}, \tag{1.3}$$

that is for each n, such that $-g\,Bo/3 > n^2$, there exists $k^*(n)$. Moreover, since $k^{*2} + n^2 = -g\,Bo/3$, the maximum growth rate λ^* is exactly the same for all k^*'s and is independent of the mode number n.

At the linear level, the above result implies that if only one critical wavenumber is excited, then the pattern is regular with a single wavenumber, while for higher values of Bond number or acceleration more than one critical wavenumber are excited such that the picture will likely become 'frustrated', cf. figure 1.1, as was discovered recently in the experimental study of the drop splash problem [11]. The frustration picture occurs due to randomness of the initial conditions, which are amplified and evolved into several superimposed patterns of different wavenumbers; accordingly, these patterns are positioned with respect to each other in a random manner.

1.2 Known approaches

The theoretical developments here deal with one-dimensional systems, i.e. on a line. This is *not* the typical form we are used to, where a data point is (x_i, y_i) and analysis determines the functional relationship between x and y. The work here is different because our data are a list of points of the form $\{x_1, \ldots, x_n\}$ where each x_i is considered a point or event of interest. With such data lying on a line, one can only measure a single quantity. Therefore, the arrangement of 1D data is the focus of analysis.

In the case of the drop splash crown, as in figure 1.1, each x_i represents the location of an individual crown spike. An example in the time domain might be flashing fireflies [3], where one would want to experimentally record the periodic flashing. Each x_i would be a time corresponding to a single flash. The problem, in both the time domain or spatial domain, is to determine the periodic structure solely from the list of events or locations.

One might simply conclude that a periodic signal should have a nearly constant intervals. Indeed, finite differences are appropriate for the case of a single frequency. However once multiple

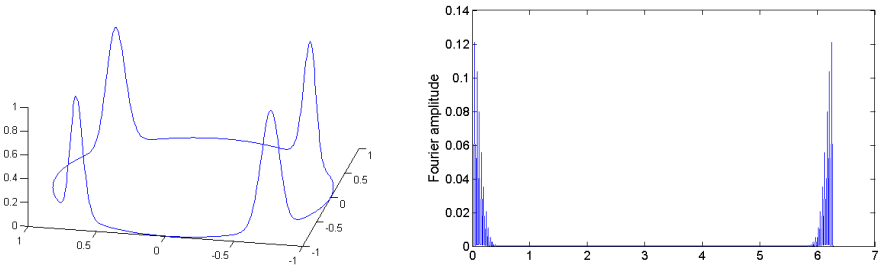

(a) Test pattern with wavenumber 4.

(b) Fourier amplitude plot.

Figure 1.3: The FT amplitudes in (b) do not identify the pattern in (a).

frequencies are present, one must account for "interference" and finite differences alone become insufficient. Using other ad hoc, "brute force", computational methods to search for patterns is not feasible because of the large number of combinations and arrangements.

1.2.1 Fourier transform

The Fourier transform (FT) is the first tool for wavenumber or frequency analysis. However, the FT is not applicable to data on a line – one cannot apply the FT to a list of numbers. Even if a hypothetical experiment measured the measured height of a crown, shown in figure 1.3(a). The FT amplitudes in figure 1.3(b) do not identify, i.e. via a spike in amplitude we would expect, the pattern with wavenumber 4. This result is not surprising because there is no base sinusoidial function to uncover; the pattern is periodic but highly nonlinear.

1.2.2 Circular statistics

The field of statistics which deals exclusively with systems on a circle is called circular statistics. Applications consist of analysis of angles and time (e.g. 0-24hrs) where the domain is

circular. Since the circle is a closed repeating domain, many standard statistical techniques are invalid. To cite a typical example: the mean of 359°, 1° and 2° is not the arithmetic mean 181° but 1° [12].

To calculate the mean of a set of angles one must separate the angles into two parts: a sine and a cosine. The sines and cosines are added up separately and the arctangent is used to get the resulting angle. This can be rephrased more compactly using complex exponentials

$$r(m) = \frac{1}{N} \sum_{n=1}^{N} e^{i\theta_n m}. \tag{1.4}$$

In dynamical systems, $r(m)$ is called the complex order parameter [13]. In the circular statistics literature, it is known as the trigonometric moment [12]. The complex order parameter is a useful diagnostic tool but its scope is to give a sense of how well ordered the system is. For the circular statistics and dynamical systems communities, a regularly spaced set is considered disordered and is not meaningful or interesting. To give an example from circular statistics: biologists measure the angles at which birds take flight. The biologist is interested in how the data are clumped, i.e. are the birds leaving in the same direction. A regular distribution of the departure angles would involve some sophisticated birds! Therefore, the circular statistics community has not considered the identification and quantification of regular patterns.

Chapter 2

Pattern identification theory

The purpose of the following theoretical development is to identify regular patterns in physical systems with O(2) symmetry. Systems with O(2) symmetry are circular systems, that is, systems which exist on the domain of a circle. For example: measurements of angles (where 0° is also 360°) and measurements of time (where 0hr is 24hr).

2.1 General terminology

We begin by introducing and defining our terminology and variables. A regular pattern is a set consisting of a union of single-wavenumber patterns. A single-wavenumber pattern is a set of elements which are regularly spaced; mathematically then, each element is a multiple of some base length, or wavelength, plus an offset or phase shift. Thus, an irregular pattern contains no regular structure and cannot be decomposed into a union of single-wavenumber patterns.

For systems with circular symmetry it is natural to consider a data point as an angle $\theta \in [0, 2\pi)$ where the angles 0 and 2π are understood to represent the same point. A single-wavenumber

pattern is described by a wavenumber k and a phase shift ϕ, illustrated in figure 2.1. Positive angles are measured (and plotted) increasing counter-clockwise from the x-axis. The spacing between two consecutive elements of a single-wavenumber pattern is called the wavelength λ and related to the wavenumber by $\lambda = 2\pi/k$.

If a single-wavenumber pattern with wavenumber n contains n elements it is said to be complete, and is not missing any elements. For more complex regular patterns consisting of multiple single-wavenumber patterns, completeness implies that no single-wavenumber is missing an element.

Expressing a regular pattern in terms of each single-wavenumber pattern constitutes a decomposition. Regular patterns, by definition, can always be decomposed into single-wavenumber patterns. If a given set can be decomposed in such a manner then it is identified as regular.

2.2 Ideal patterns

We begin with the simplest case, the "ideal pattern" which is considered to be free from experimental scatter or error. The ideal case will form the basis for more general and complex cases developed later. Indeed, the ideal pattern contains many subtleties itself and requires careful attention.

2.2.1 Definitions

Definition 1 (Ideal single-wavenumber pattern)**.** Let $\Theta = \{\theta_1, \ldots, \theta_k\}$ be a set of k elements. If $\Theta = \{\theta_n \in [0, 2\pi) \,|\, \theta_n = n\lambda + \phi, \text{ for } n = 0, \ldots, k-1\}$, where the wavelength $\lambda = 2\pi/k$ and the phase shift $\phi \in [0, \lambda)$, then Θ is an *ideal single-wavenumber pattern* and may be represented more compactly

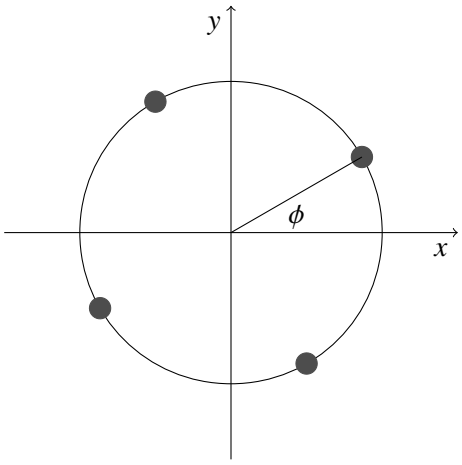

Figure 2.1: An ideal single-wavenumber pattern, $\Theta(4, \phi)$, with wavenumber 4 and phase shift ϕ.

as $\Theta(k, \phi)$.

An ideal regular pattern is a set which can be decomposed into ideal single-wavenumber patterns. Let $\mathbf{\Theta}$ be the set containing all elements of interest and $\Theta^{(i)}$ be the i^{th} ideal single-wavenumber pattern, we may now define an ideal regular pattern.

Definition 2 (Ideal regular pattern)**.** If $\mathbf{\Theta} = \bigcup_{i=1}^{m} \Theta^{(i)}(k_i, \phi_i)$, where m is the least number of ideal single-wavenumber patterns necessary, then $\mathbf{\Theta}$ is an *ideal regular pattern*.

Remark 1. In general, the decomposition of an ideal regular pattern into ideal single-wavenumber patterns is not unique. Hence, for uniqueness it is necessary to describe a regular pattern using the least number of single-wavenumber patterns. Further discussion of this fact may be found in §2.4 on regular patterns with overlaps.

Example 2.2.1. To clarify the terminology introduced above, consider as an example figure 2.1. Plotted are the angles from the set $\mathbf{\Theta} = \{\phi, \pi/2 + \phi, \pi + \phi, 3\pi/2 + \phi\}$. By inspection we see the

wavenumber $k = 4$, the wavelength $\lambda = \pi/2$, and the phase shift ϕ. Indeed, this set is a single-wavenumber pattern because $\mathbf{\Theta} = \Theta(4, \phi) = \left\{\theta_n \in [0, 2\pi) \,|\, \theta = n\frac{\pi}{2} + \phi, \text{ for } n = 0, 1, 2, 3\right\}$.

End of example 2.2.1

One key to uncovering the regular decomposition of a set $\mathbf{\Theta} = \{\theta_1, \ldots, \theta_N\}$ with N elements involves the construction of a difference matrix $\Delta\mathbf{\Theta}$ which consists of differences between all pairs of elements in that set. This is implemented using a difference operator Δ where $\Delta\mathbf{\Theta}$ is an $N \times N$ skew-symmetric matrix, with elements

$$\Delta\mathbf{\Theta}_{ij} = \theta_i - \theta_j. \tag{2.1}$$

Remark 2. The difference matrix $\Delta\mathbf{\Theta}$ contains $\frac{N^2-N}{2} = \frac{N!}{(N-2)!2!} = \binom{N}{2}$ possible unique entries. Additionally, if $\mathbf{\Theta}$ is sorted in ascending order then the lower triangular half of $\Delta\mathbf{\Theta}$ contains all the positive difference combinations.

2.2.2 Identification of ideal patterns without overlaps

Theorem 1. *If a given ideal regular pattern is complete and without overlaps, then there exists an algorithm which identifies it.*

Proof. Let us demonstrate the existence of at least one algorithm which decomposes any given ideal regular pattern, which is complete and without overlaps into ideal single-wavenumber patterns. Let $\mathbf{\Theta}$ be an ideal regular pattern with N elements containing m ideal single-wavenumber patterns, that is

$$\mathbf{\Theta} = \bigcup_{i=1}^{m} \Theta^{(i)}(k_i, \phi_i), \tag{2.2}$$

where $\Theta^{(i)} \bigcap \Theta^{(j)} = \emptyset$ if $i \neq j$. In order to begin decomposing the given set $\mathbf{\Theta}$ into ideal single-wavenumber patterns $\Theta^{(i)}(k_i, \phi_i)$, we first attempt to identify the wavelength λ of ideal single-wavenumber patterns with wavenumber $2\pi/\lambda$. Let us consider a difference between two elements of $\mathbf{\Theta}$

$$\Delta\mathbf{\Theta}_{ij} = \theta_i - \theta_j = (n\lambda_i + \phi_i) - \left(n'\lambda_j + \phi_j\right), \tag{2.3}$$

for some $n, n' \in \mathbb{Z}^+$. We arrive at equation (2.3) based on the fact that θ_i and θ_j are each members of *some* ideal single-wavenumber pattern. Any pair of elements belong either to the same single-wavenumber pattern or to different single-wavenumber patterns. Should two elements *happen* to belong to the same single-wavenumber pattern, i.e. if $\theta_i, \theta_j \in \Theta^{(i)}$, then $\lambda_i = \lambda_j$ and $\phi_i = \phi_j$. Thus equation (2.3) becomes

$$\Delta\mathbf{\Theta}_{ij} = (n - n')\,\lambda_i. \tag{2.4}$$

Although n, n' are unknown indicies, certainly it is possible that $n - n' \in \mathbb{Z}^+$. Equation (2.4) affirms the physical intuition that the spacing between elements in an ideal single-wavenumber pattern are multiples of the wavelength of that pattern. In particular, for a single-wavenumber pattern of wavenumber k containing k elements, we should expect to find $\binom{k}{2} = \frac{k!}{2!(k-2)!}$ positive entries in the difference matrix $\Delta\mathbf{\Theta}$. Given λ_i, equation (2.4) allows one to form a set of elements from $\Delta\mathbf{\Theta}_{ij}$, which may belong to a single-wavenumber pattern with wavelength λ_i.

The set of elements which are spaced by multiples of λ_i requires further consideration. Two complications can arise: it may be that "pathological" phase shifts give rise to spurious pairs of elements, or there may be multiple single-wavenumber patterns with the same wavenumber and hence the same wavelength. This first step cannot distinguish between spurious cases and the single-wavenumber patterns we wish to identify. By trial and error, possible single-wavenumber patterns

are considered beginning with the largest possible wavenumber, the total number of elements in $\mathbf{\Theta}$, and decreasing incrementally. Starting with largest wavenumber ensures that the fewest number of single-wavenumber patterns will be used in the decomposition. As single-wavenumber patterns are identified, they are removed and the process iterates until every element of $\mathbf{\Theta}$ belongs to a unique single-wavenumber pattern.

As a result, an algorithm for the identification of ideal regular patterns without overlaps involves the following steps:

1. Given $\mathbf{\Theta} = \{\theta_1, \ldots, \theta_N\}$, compute $\Delta\mathbf{\Theta}$.

2. Let the wavenumber $k = N$, which gives the wavelength $\lambda = 2\pi/k$.

3. Find all indices i, j for which $\Delta\mathbf{\Theta}_{ij} = n\lambda$ for any possible $n \in \mathbb{N}$.

4. From indices i, j, place the corresponding θ_i, θ_j, into a new set Θ' with L members.

5. Partition Θ' into blocks of ideal single-wavenumber patterns with wavenumber k according to phase shift with the following substeps:

   (a) Given $\Theta' = \left\{\theta'_1, \ldots, \theta'_L\right\}$ in ascending order, $\theta'_1 < \theta'_2 < \ldots < \theta'_L$.

   (b) Let us assume $\theta'_1 = \theta_0^{(1)} \in \Theta^{(1)}$, which gives $\phi_1 = \theta'_1$ and the first ideal single-wavenumber pattern: $\Theta^{(1)}(k, \phi_1)$.

   (c) If $\Theta^{(1)} \subseteq \Theta'$, then subtract it from the set of points: $\Theta' \rightarrow \Theta' \setminus \Theta^{(1)}$ and repeat by returning to substep (a).

   (d) If $\Theta^{(1)} \nsubseteq \Theta'$, then return to substep (b) for $\theta'_1 \rightarrow \theta'_2$.

   (e) Once Θ' is empty or all possible θ' have been tried, the partitioning is complete.

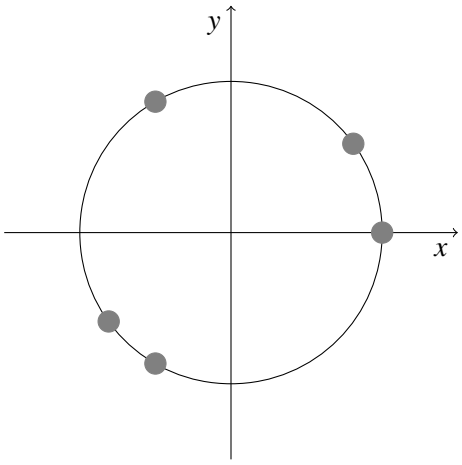

Figure 2.2: An ideal regular pattern consisting of two ideal single-wavenumber patterns: $\Theta(3,0) \bigcup \Theta(2,\pi/5)$.

6. Once $\boldsymbol{\Theta}$ is empty the procedure is complete, otherwise repeat the above steps for $\boldsymbol{\Theta} \rightarrow \boldsymbol{\Theta} \setminus \Theta^{(i)}$ and $k \rightarrow k-1$.

By applying the above algorithm one identifies the ideal regular pattern, which may potentially consist of several ideal single-wavenumber patterns. □

We demonstrate the implementation of the algorithm in the example below:

Example 2.2.2. The algorithm will now be demonstrated for ideal pattern in figure 2.2. These angles, $\boldsymbol{\Theta} = \{0, \pi/5, 2\pi/3, 6\pi/5, 2\pi/3\}$, could be data we want to identify as regular. The first step requires the calculation of the difference matrix $\Delta\boldsymbol{\Theta}$

$$\Delta\boldsymbol{\Theta} = \begin{pmatrix} 0 & -\pi/5 & -2\pi/3 & -6\pi/5 & -4\pi/3 \\ \pi/5 & 0 & -7\pi/15 & -\pi & -17\pi/15 \\ 2\pi/3 & 7\pi/15 & 0 & -8\pi/15 & -2\pi/3 \\ 6\pi/5 & \pi & 8\pi/15 & 0 & -8\pi/15 \\ 4\pi/3 & 17\pi/15 & 2\pi/3 & 8\pi/15 & 0 \end{pmatrix}. \tag{2.5}$$

Since there are a total of 5 elements in $\boldsymbol{\Theta}$, we begin with the largest possible wavenumber $k = 5$ and the wavelength $\lambda = 2\pi/5$. There is one entry in $\Delta\boldsymbol{\Theta}$ which is a positive multiple of $2\pi/5$, therefore $\Theta' = \{0, 6\pi/5\}$. One single-wavenumber pattern is formed because $\phi = 6\pi/5$ is not possible for a pattern with $\lambda = 2\pi/5$. In any case, the single-wavenumber pattern would have five elements and cannot be a subset of Θ'. The wavenumber test drops to $k = 4$.

There is one entry in $\Delta\boldsymbol{\Theta}$ which is a multiple of $\lambda = \pi/2$. The two respective angles are placed in the temporary set $\Theta' = \{0, \pi\}$. The attempted ideal-single wavenumber pattern $\Theta(4, 0)$ is not a subset of Θ'. The next wavenumber to test is 3.

The search for multiples of wavelength $2\pi/3$ corresponding to wavenumber 3, forms the set $\Theta' = \{0, 2\pi/3, 4\pi/3\}$. This time, $\Theta^{(1)}(3, 0)$ is a subset of Θ'. The partitioning substeps completed, the wavenumber drops to 2 and the successfully identified single-wavenumber pattern $\Theta^{(1)}(3, 0)$ is subtracted from $\boldsymbol{\Theta}$.

For $k = 2$ there is only one positive entry in the new difference matrix $\boldsymbol{\Theta}$

$$\Delta\boldsymbol{\Theta} = \begin{pmatrix} 0 & -\pi \\ \pi & 0 \end{pmatrix}. \tag{2.6}$$

This one entry is equal to the wavelength $\lambda_2 = \pi$. The first element, $\theta'_1 = \pi/5$ gives the phase shift $\phi_2 = \pi/5$ of the second single-wavenumber pattern $\Theta^{(2)}(2, \pi/5)$. Every element of the given set belongs to one of two single-wavenumber patterns and the decomposition is complete.

End of example 2.2.2

2.3 Regular patterns with scatter

A natural generalization of ideal patterns is to consider non-ideal patterns. Indeed, any experimentally determined quantity necessarily has an uncertainty attached to it. As such, the following development is more immediately applicable to actual measured data. We introduce such non-ideal patterns by allowing deviations, i.e. residuals, from the ideal case. Hence, a regular pattern with scatter is "scattered" about the ideal regular pattern by letting ϵ_i be the deviation of θ_i from ideal case. A natural assumption is that the magnitude of the uncertainties $|\epsilon_i|$ is bounded by some constant δ. Such patterns are called regular with scatter, where the amount of scatter is parameterized by δ.

2.3.1 New notation for patterns with scatter

Definition 3 (Single-wavenumber pattern with scatter)**.** Let $\Theta = \{\theta_1, \ldots, \theta_k\}$ be a set with k elements. If $\Theta = \{\theta_n \in [0, 2\pi) \,|\, \theta_n = n\lambda + \phi + \epsilon_n, \text{ for } n = 0, \ldots, k-1, |\epsilon_n| \leq \delta\}$, where the wavelength $\lambda = 2\pi/k$, the phase shift $\phi \in [0, \lambda)$ and the scatter $\delta \in [0, \lambda/2)$, then Θ is a *single-wavenumber pattern with scatter* and may be represented as $\Theta(k, \phi, \delta)$.

Figure 2.3 illustrates the correspondence between the two ways of viewing the same pattern. On the left is a circle where the point θ_i is shifted by ϵ_i from the ideal location. On the right is a new plot of (n, θ). The linear relationship represents the ideal limit where $\delta \to 0$. The graphical representation of a regular pattern naturally allows for scatter and phase shifts. The phase shift is the y-intercept of the line. We can apply standard error analysis [14] by considering $\theta = \theta_1, \ldots, \theta_N$ as a series of measurements which ideally fall a line described by $\theta = \lambda n + \phi$. Note that one can only plot (n, θ_n) for a given set $\boldsymbol{\Theta}$ *after* the regular pattern with scatter has been identified.

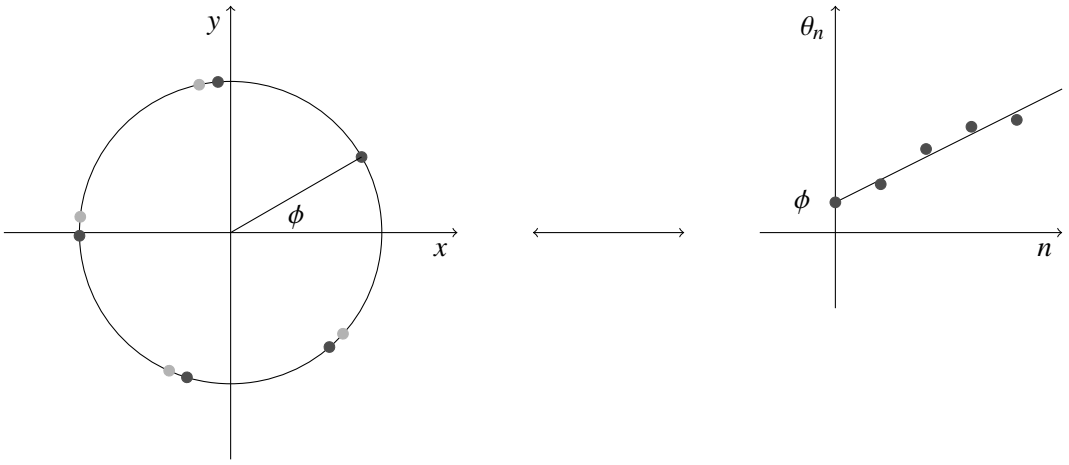

Figure 2.3: Representing a circular pattern on a graph: the lightly shaded dots indicate the ideal single-wavenumber pattern, the dark points are plotted on the right as coordinates (n, θ_n), where the line represents the ideal linear relationship $\theta = n\lambda + \phi$, ϵ_n is the residual between the line and the plotted point.

The "ideal regime" for patterns with scatter is a somewhat specific set of conditions under the broader spectrum of regular patterns with scatter. In the ideal regime, patterns with scatter may be identified using a generalized version of the ideal algorithm; the ideal algorithm is recovered for $\delta \to 0$. The condition for a given pattern to be in the ideal regime is two elements are not closer than twice the scatter δ. As a consequence, this means than the smallest allowable wavelength is $\lambda = 2\delta$. By spacing the elements into what amounts to islands of uncertainty, we avoid the ambiguous case where two points lie within the scatter radius and effectively overlap.

From a theoretical perspective two conditions, spacing and completeness are enough to avoid complicating cases. However, from an experimental perspective the amount of scatter itself is interesting. As such, a dimensionless scatter ratio $2\delta/\lambda$ is a useful parameter to quantify the relative amount of scatter.

2.3.2 Identification of regular patterns with scatter

Theorem 2. *If a given regular pattern with scatter is complete and in the ideal regime, where no two elements are closer than twice the scatter, then there exists an algorithm which identifies it.*

Proof. We will again demonstrate the existence of an algorithm which identifies regular patterns with scatter by providing the decomposition into single-wavenumber patterns with scatter. Let $\mathbf{\Theta}$ be a regular pattern with N elements which can be partitioned into m single-wavenumber patterns with scatter δ. In the ideal regime, the single-wavenumber patterns are separated such that $\Theta^{(i)} \bigcap \Theta^{(j)} = \emptyset$ if $i \neq j$. As for the case without scatter, we begin by considering a difference between two elements of $\mathbf{\Theta}$

$$\Delta\mathbf{\Theta}_{ij} = \theta_i - \theta_j = (n\lambda_n + \phi_n + \epsilon_n) - (n'\lambda_{n'} + \phi_{n'} + \epsilon_{n'}), \tag{2.7}$$

for some indicies n, n'. Like the ideal case before, equation (2.7) may be simplified if θ_i and θ_j belong to the same single-wavenumber pattern with scatter. That is, $\theta_i, \theta_j \in \Theta^{(k)}$

$$\Delta\mathbf{\Theta}_{ij} = (n - n')\lambda + \epsilon_n + \epsilon_{n'}. \tag{2.8}$$

By assumption $\epsilon_n, \epsilon_{n'}$ are both bounded by constant δ. This relation gives

$$|\Delta\mathbf{\Theta}_{ij} - (n - n')\lambda| \leq 2\delta. \tag{2.9}$$

Equation (2.9) is the exact analogy to equation (2.4) in the ideal case before, with the difference being that the scatter parameter δ introduces an inequality. Indeed, the ideal equality is recovered in the limit $\delta \to 0$. In the ideal regime, the analysis is simple and no "pathological" cases need be considered because the points are spaced as if the pattern were ideal. With the modification of the equality to an inequality in step 3 below, the algorithm is identical to the algorithm presented for ideal regular patterns.

As a result, the algorithm presented below identifies regular patterns if they are complete and without overlaps:

1. Given $\mathbf{\Theta} = \{\theta_1, \ldots, \theta_N\}$ and δ, compute $\Delta\mathbf{\Theta}$.

2. Let the wavenumber $k = N$, which gives the wavelength $\lambda = 2\pi/k$.

3. Find all indicies i, j for which $|\Delta\mathbf{\Theta}_{ij} - n\lambda_k| \leq 2\delta$ for any possible $n \in \mathbb{N}$.

4. From indicies i, j, place the corresponding θ_i, θ_j into a new set Θ'.

5. From indices i, j, place the corresponding θ_i, θ_j, into a new set Θ' with L members.

6. Partition Θ' into blocks of single-wavenumber patterns with scatter δ and wavenumber k according to phase shift with the following substeps:

   (a) Given $\Theta' = \left\{\theta'_1, \ldots, \theta'_L\right\}$ in ascending order, $\theta'_1 < \theta'_2 < \ldots < \theta'_L$.

   (b) Let us assume $\theta'_1 = \theta_0^{(1)} \in \Theta^{(1)}$, which gives $\phi_1 = \theta'_1$ and the first single-wavenumber pattern: $\Theta^{(1)}(k, \phi_1)$.

   (c) If $\Theta^{(1)} \subseteq \Theta'$, then subtract it from the set of points: $\Theta' \to \Theta' \setminus \Theta^{(1)}$ and repeat by returning to substep (a).

   (d) If $\theta^{(1)} \nsubseteq \Theta'$, then return to substep (b) for $\Theta'_1 \to \Theta'_2$.

   (e) Once Θ' is empty or all possible θ' have been tried, the partitioning is complete.

7. Once Θ is empty the procedure is complete, otherwise the above steps for $\Theta \to \Theta \setminus \Theta^{(i)}$ and $k \to k - 1$.

The above algorithm identifies regular patterns with scatter in the ideal regime. □

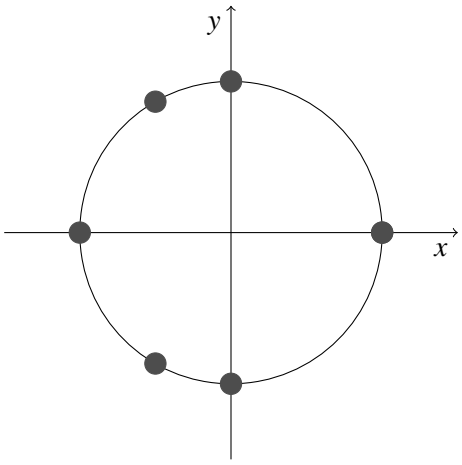

Figure 2.4: Two overlapping single-wavenumber patterns with wavenumbers 3 and 4 which share the element $\theta = 0$.

The generalization, therefore, from ideal patterns to patterns with scatter is straightforward in the ideal regime.

2.4 Patterns with overlaps

Until now, we have only considered regular patterns when no overlapping single-wavenumber patterns may occur. Figure 2.4 illustrates an ideal regular pattern with overlaps consisting of two single-wavenumber patterns which have one element in common. For this case, the element $\theta = 0$ is shared between the single-wavenumber pattern $\Theta(3, 0)$ and $\Theta(4, 0)$. Due to the fact that overlapping elements are "double-counted," a regular pattern with overlaps has fewer elements than the sum of wavenumbers of the constituent single-wavenumber patterns. The difficulties introduced by overlaps warrant a theoretical treatment for ideal case which may later be generalized to patterns with scatter. The presence of overlaps in a regular pattern demands a full understanding of the nature of single-wavenumber patterns which begins with a discussion of "subpatterns."

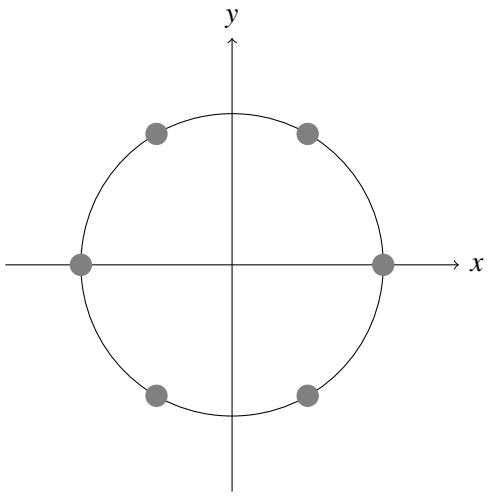

Figure 2.5: An ideal single-wavenumber pattern $\Theta(6, 0)$.

2.4.1 Subpatterns of single-wavenumber patterns

A single-wavenumber pattern may be described as a union of smaller "subpatterns" in a manner analogous to factoring a natural number; where the single-wavenumber pattern is decomposed into subpatterns. A subpattern is simply another single-wavenumber pattern with a smaller wavenumber which is a subset of the larger single-wavenumber pattern in consideration. This idea of factoring will prove useful when distinguishing patterns for the case of patterns with overlaps. We now clarify these ideas with an example.

Example 2.4.1. Referring to figure 2.5 where $\Theta(6, 0) = \left\{\theta_n \in [0, 2\pi) | \, \theta = \frac{n\pi}{3}, \text{ for } n = 0, \ldots, 5\right\}$, we can make the following observation for a single-wavenumber pattern with wavenumber 6: it can be grouped into two sets of single-wavenumber patterns with wavenumber 3, or into three sets of single-wavenumber patterns with wavenumber 2. Once that observation is made, it is not difficult

to come up with the exact expressions:

$$\Theta(6,0) = \Theta^{(1)}(3,0) \bigcup \Theta^{(2)}(3,\pi/3)\,, \tag{2.10}$$

$$= \Theta^{(3)}(2,0) \bigcup \Theta^{(4)}(2,\pi/3) \bigcup \Theta^{(5)}(2,2\pi/3)\,. \tag{2.11}$$

End of example 2.4.1

Theorem 3. *Any ideal single-wavenumber pattern* $\Theta(N,\phi)$ *may be expressed as a union of ideal single-wavenumber patterns of wavenumber* p *where* p *divides* N

$$\Theta(N,\phi) = \bigcup_{i=1}^{N/p} \Theta^{(i)}\left(p, \phi + \lambda_N(i-1)\right)\,. \tag{2.12}$$

Proof. Two sets are equal if every element in the set on the right-hand side is in the set on the left-hand side, and vice-versa. We begin by expanding the right-hand side by considering the n^{th} element of the i^{th} single-wavenumber pattern.

$$\theta_n^{(i)} = \frac{2\pi n}{p} + \phi + \lambda_N(i-1) = \frac{2\pi n}{p} + \phi + \frac{2\pi(i-1)}{N}\,. \tag{2.13}$$

Letting N and ϕ be given, we take the general element $\theta_{n'}^{(i)}$ on the right-hand side, and assume it is equal to some θ_n on the left-hand side

$$\theta_n = \theta_{n'}^{(i)}\,, \tag{2.14}$$

$$\frac{2\pi n}{N} + \phi = \frac{2\pi n'}{p} + \phi + \frac{2\pi(i-1)}{N}\,, \tag{2.15}$$

$$\frac{n}{N} = \frac{n'}{p} + \frac{i-1}{N}\,. \tag{2.16}$$

Th derive conditions under which the assumption is true, we rearrange equation (2.16) into

$$n - n'\frac{N}{p} - i + 1 = 0\,. \tag{2.17}$$

From equation (2.17), we may deduce our desired result. First, note that n and n' are indicies, which by definition are non-negative integers. N is the wavenumber of the single-wavenumber pattern which is a positive integer. Since every variable in the equation is an integer, we can only use equation (2.17) to translate between θ_n and $\theta^{(i)}_{n'}$ if N/p is an integer as well. That is, given some fixed N – and p which divides N, we can find the n'^{th} element of the i^{th} subpattern equal to the n^{th} element of the single-wavenumber patter. Or, conversely, given the n'^{th} element of the i^{th} subpattern we can find the n^{th} element of the single-wavenumber pattern. Therefore, the two sets are equal. □

2.4.2 Identification of ideal patterns with overlaps

We now consider ideal regular patterns, which may contain overlapping ideal single-wavenumber patterns. Assuming that each single-wavenumber pattern, which constitutes the regular pattern, is complete, i.e. each contains the same number of elements as the wavenumber, then this is the most general case for ideal patterns.

Theorem 4. *If a given ideal regular pattern – possibly containing overlaps – is complete, then an algorithm exists which identifies it.*

Proof. We will again demonstrate the existence of an algorithm which identifies ideal regular patterns, which potentially consists of overlapping ideal single-wavenumber patterns. Accommodating the presence of overlaps requires only a few modifications of the original algorithm. The main modification is to note that a given element $\theta_i \in \mathbf{\Theta}$ may belong to multiple single-wavenumber patterns. Therefore, subtracting single-wavenumber patterns as they are identified removes other equally valid single-wavenumber patterns. One mechanism to avoid this problem is to test for and identify all possible single-wavenumber patterns with wavenumbers ranging from N to 2 without

removing single-wavenumber patterns as they are each identified. From theorem 3 on subpatterns presented above, finding the redundant subpatterns of a single-wavenumber pattern is trivial. Once subpatterns are removed, which is accomplished in step 7, all that remains are the largest possible single-wavenumber patterns, which constitute the decomposition of the ideal regular pattern.

As a result, an algorithm for the identification of complete ideal regular patterns involves the following steps:

1. Given $\mathbf{\Theta} = \{\theta_1, \ldots, \theta_N\}$, compute $\Delta\mathbf{\Theta}$.

2. Let the wavenumber $k = N$, which gives the wavelength $\lambda = 2\pi/k$.

3. Find all indicies i, j for which $\Delta\mathbf{\Theta}_{ij} = n\lambda$ for any possible $n \in \mathbb{N}$.

4. From indicies i, j place the corresponding θ_i, θ_j into a new set Θ' with L members.

5. Partition Θ' into blocks of ideal single-wavenumber patterns with wavenumber k according to phase shift.

   (a) Given $\Theta' = \left\{\theta'_1, \ldots, \theta'_L\right\}$ in ascending order, $\theta'_1 < \theta'_2 < \ldots < \theta'_L$.

   (b) Let us assume $\theta'_1 = \theta_0^{(1)} \in \Theta^{(1)}$, which gives $\phi_1 = \theta'_1$ and the first ideal single-wavenumber pattern: $\Theta^{(1)}(k, \phi_1)$.

   (c) If $\Theta^{(1)} \subseteq \Theta'$, then subtract it from the set of points: $\Theta' \rightarrow \Theta' \setminus \Theta^{(1)}$ and repeat by returning to substep (a).

   (d) If $\Theta^{(1)} \nsubseteq \Theta'$, then return to substep (b) for $\theta'_1 \rightarrow \theta'_2$.

   (e) Once Θ' is empty or all possible θ' have been tried, the partitioning is complete.

6. Repeat the procedure for $k = N - 1, N - 2, \ldots, 2$.

7. Considering all possible $\Theta^{(j)}$ and $\Theta^{(m)}$, remove any $\Theta^{(m)}$ for which $\Theta^{(m)} \subset \Theta^{(j)}$.

□

Example 2.4.2. Here we demonstrate how the modifications made to the algorithm without overlaps enable a relatively straightforward mechanism for handling a regular pattern with overlaps. Referring to figure 2.4, the set of angles given is $\mathbf{\Theta} = \Theta(4,0) \bigcup \Theta(3,0)$. The result of steps 1-6 is a group of identified single-wavenumber patterns: $\Theta^{(1)}(4,0), \Theta^{(2)}(3,0), \Theta^{(3)}(2,0), \Theta^{(4)}(2,\pi/2)$. From theorem 3, it is clear that third and fourth patterns are subpatterns of the first single-wavenumber pattern. Therefore, these are removed in step 7 and the remaining decomposition is the desired one consisting of two single-wavenumber patterns with wavenumbers three and four.

End of example 2.4.2

2.5 Incomplete patterns

We now consider the case of incomplete patterns, that is, patterns which are missing points but are otherwise regular. Incomplete patterns suffer from a problem of definition because any given regular pattern can be considered to be the result of a larger pattern missing the appropriate elements. Another problem inherent in incomplete patterns is that they are not known to be incomplete until *after* they are identified. We illustrate these complexities with an example:

Example 2.5.1. We consider a single-wavenumber pattern $\Theta(4,\phi)$ in figure 2.6(a), and remove elements and consider whether the pattern is identifiable. For each case, we assume the pattern is regular – and *may* be incomplete. To identify an incomplete pattern, elements are added such

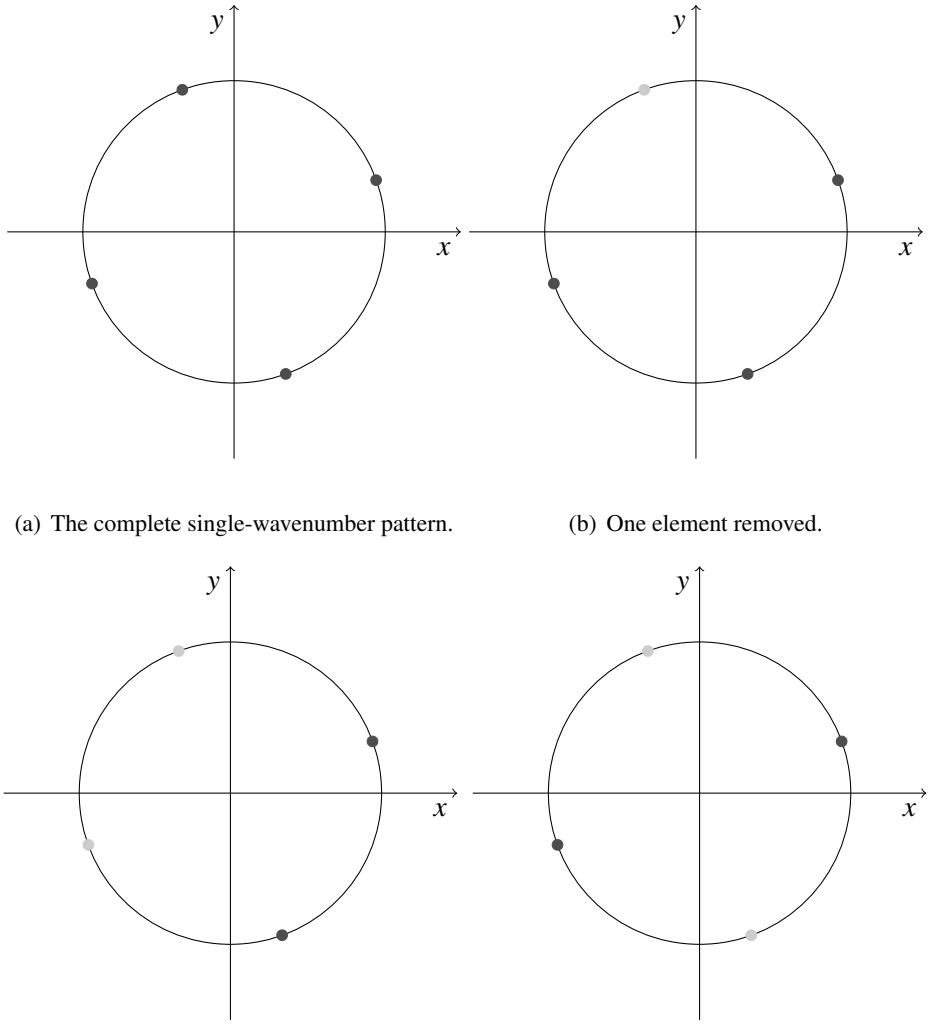

(a) The complete single-wavenumber pattern.

(b) One element removed.

(c) Two elements removed.

(d) Two elements removed.

Figure 2.6: A series of incomplete single-wavenumber patterns: (a) the complete single-wavenumber pattern with wavenumber 4, (b) the incomplete single-wavenumber pattern is identifiable, (c) the incomplete pattern is still identifiable, (d) the given pattern is identified as a single-wavenumber pattern with wavenumber 2 and cannot be identified as incomplete.

that a regular pattern is completed. Naturally, we add no more elements than necessary, thereby completing the smallest possible regular pattern.

There is one combination where one element is removed, as shown in figure 2.6(b). This incomplete pattern is identifiable because the grayed element is simply added, thereby making a complete single-wavenumber pattern.

There are two ways to remove two elements. Figure 2.6(c) shows the result if two consecutive elements are removed. In this case, the incomplete pattern may be identified because the two grayed elements may be added back to make a single-wavenumber pattern with wavenumber 4.

The other case where two elements are removed, cf. figure 2.6(d), is when non-adjacent elements are removed. In this case the "incomplete" pattern is just a single-wavenumber pattern with wavenumber 2! Therefore, the incomplete pattern is not identifiable. The key distinction in this case is that the removed elements constitute a subpattern of the single-wavenumber pattern.

End of example 2.5.1

The example presented above leads one to cautiously consider incomplete patterns. A useful definition of an incomplete pattern is the one which is "well-defined." That is, among the various ways to make a pattern incomplete (by removing combinations of elements), the incomplete pattern needs to be identified with the properties of a unique regular pattern. In other words, if we make a regular pattern incomplete by removing elements – we should be able to put it back together!

Definition 4. An *incomplete regular pattern* Θ^I is a regular pattern, Θ^R, minus a set of subtracted points Θ^- where $\Theta^- \subset \Theta^R$

$$\Theta^I(k, \phi) = \Theta^R(k, \phi) \setminus \Theta^-. \tag{2.18}$$

Claim 1. If Θ^{-} is not regular, i.e. does not contain any single-wavenumber patterns, then $\Theta^{I}(k, \phi)$ has the same properties as Θ^{R} and is well-defined among all possible Θ^{-}.

Chapter 3

Example of application: the drop splash problem

The drop splash problem has fascinated scientists and the public with the formation of patterns observed for a wide variety of conditions. As such, it is well documented and the subject of numerous studies. However, given the complexity of the problem, most studies are experimental and empirical. In particular, many studies offer qualitative observations of images. The difficulty of obtaining data from high-speed photography, i.e. position or velocity, has hampered the quantitative study of the intriguing patterns formed during a drop splash event.

Here, we present a new experimental setup and method for the purpose of quantitatively studying the patterns generated in the drop splash. The newly developed pattern identification theory and experimental methodology are demonstrated in the application to the data generated by two drop splash events; we study a regular pattern and an irregular pattern.

3.1 Background

There exist a range of conditions which may fall under the category of "drop splash". This study focuses on the regime where a liquid droplet impacts a wetted surface. The impact energy of the droplet is moderate and the film thickness is on the order of the droplet diameter. The physical parameters correspond to a droplet diameter of $5mm$, a film thickness of $1mm$, and a drop height of about $20cm$. The liquid used in this study is milk, which constitutes the film as well as the drop.

To gain an understanding of the governing parameters of the drop splash problem, we consider dimensional analysis using the Buckingham Pi theorem. Noting that the film and droplet are formed using the same liquid, the physically relevant parameters are the liquid density ρ, dynamic viscosity μ, surface tension σ, droplet size or diameter d, film size or thickness h and the drop height H. The properties of air are neglected because the difference between the density of air and water or milk is large and drag is negligible, i.e. we expect the same results if the experiment were repeated in vacuum. The Ohnesorge number $Oh = \mu/\sqrt{\sigma\rho d}$, which measures the ratio of viscous to capillary forces, is small and therefore viscosity effects are negligible. The two remaining forces which dominate are surface tension and gravity. Hence, the two dimensionless variables governing the problem are the Weber numbers of the droplet and film We_{drop} and We_{film}, which are the ratios of the inertia of the drop to surface tension and the inertia of the film to surface tension, respectively. Since drag effects are negligible, the velocity at impact is $v = \sqrt{2gH}$, where H is the drop height. Therefore the Weber numbers are $We_{\text{drop}} = \rho v^2 d/\sigma = 2\rho g H d/\sigma$ and likewise for the film, $We_{\text{film}} = 2\rho g h d/\sigma$, where h is the film thickness. Note that $We_{\text{film}} = (h/d)\, We_{\text{drop}}$. The ratio of the droplet diameter to film thickness is called the inertia ratio $\alpha = d/h$. Returning the the Buckingham Pi theorem, the expected number of dimensionless variables is 2 which is the 5 governing param-

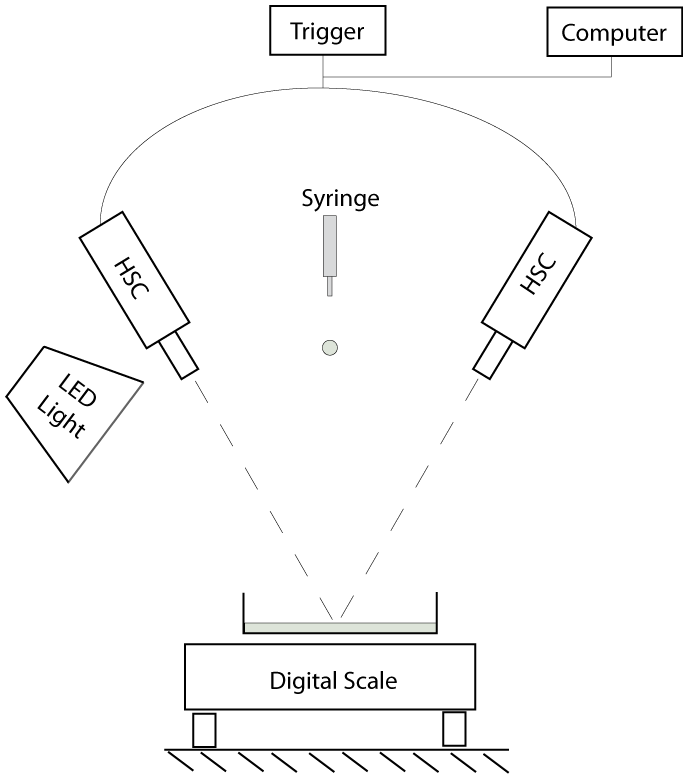

Figure 3.1: Schematic of the experimental setup consisting of an LED bulb, precision balance, two synchronized high-speed cameras, a trigger for the cameras, and a dish holding the film.

eters (neglecting viscosity) less the 3 standard measurement quantities (mass, length, time). These two dimensionless variables are accounted for with the Weber number of the droplet and the inertia ratio α. The experimental variables, for a given fluid and syringe, are the film thickness h and drop height H.

3.2 Experimental setup and procedure

The experimental setup used to capture the event is slightly modified from that used in the work [11]. The schematic in figure 3.1 contains all the key components necessary to perform the experiment and can be "decomposed" into two groups of components. The first group is responsible

for measuring the physical parameters and generating the drop splash and is identical to the previous setup used in [11]. The second group of equipment is used to capture the event, this is different from previous work.

We now describe the first group which measure the conditions of the drop splash. To generate the droplet, a pump pushes liquid through a syringe. The pump is run at a consistent low speed ensuring that droplet formation is uniform. The syringe is positioned above a petri dish using a linear actuator. The film is held in a petri dish atop a precision digital balance (Ohaus EP612C) which is used to measure the film thickness gravimetrically, i.e. by measuring the mass of the fluid one can calculate the film thickness.

The second group of components serve to capture the drop splash event. Since the whole drop splash event is over in a fraction of a second, high-speed cameras are necessary to capture the dynamics. Also, since we are interested in the structure of the crown in space, we appeal to 3D photography. The setup in figure 3.1 shows how two high-speed cameras (Phantom 5.1 and 5.2) are positioned to generate a stereo video of the event. The cameras need to be connected to each other and to a trigger to ensure that the stereo videos are synchronized, i.e. so that each of pair of frames correspond to the same time.

3.2.1 Stereo camera calibration and triangulation

The practice of making physical measurements using images, known as photogrammetry, is over a century old; the historical development of camera models and calibration techniques may be found in [4]. With the introduction of digital cameras (and personal computers), an important area of research has been to allow a simple, robust, and automated means of camera calibration. The result of a "camera calibration" is a model of the camera which translates between a point in an

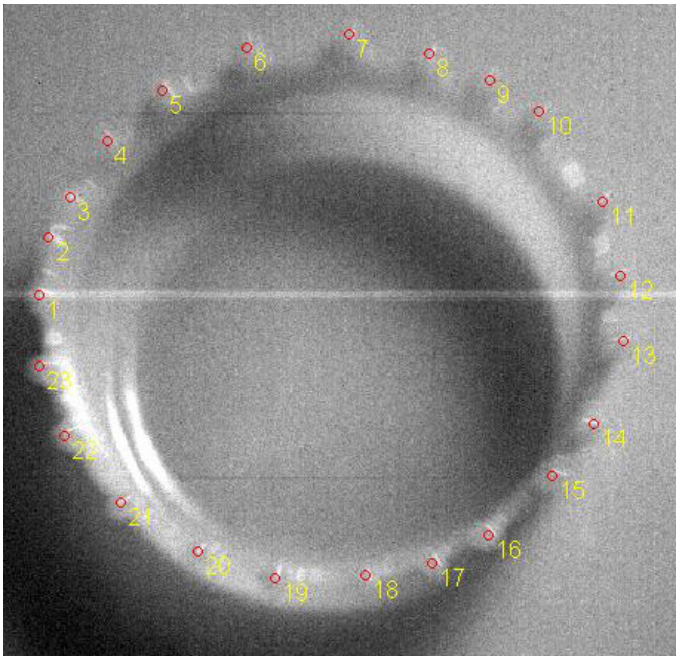

(a) Left image.

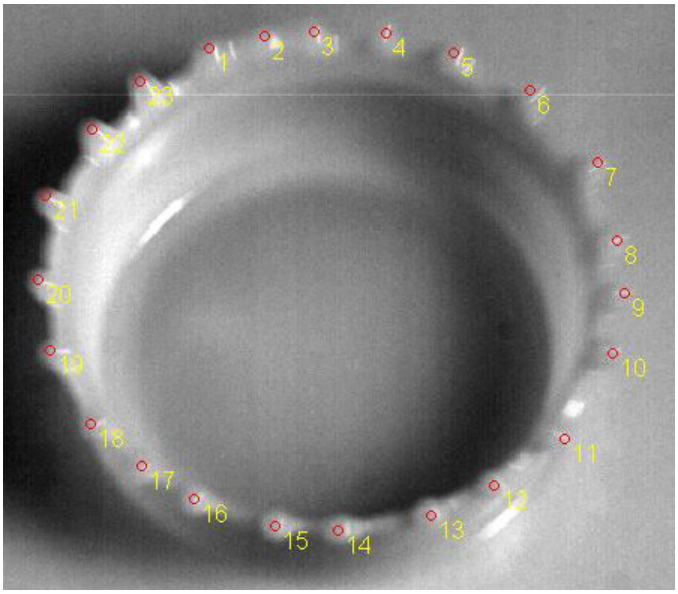

(b) Right image.

Figure 3.2: Stereo images of a drop splash crown with corresponding spikes labeled by number.

image and the light ray that is projected to that point. Beginning with the seminal work by Tsai in 1987 [15], steady progress has been made towards the passive calibration of off-the-shelf cameras [8, 17]. That is, calibration procedures which use natural lighting and do not require any internal information about the camera (such as its focal length). Jean-Yves Bouguet has implemented the latest research, including his thesis work [1], into a toolbox written in Matlab called the "Camera Calibration Toolbox for Matlab" [2].

Stereo triangulation, i.e. the determination of a coordinate in 3D from a pair of images, is possible once a stereo calibration has been performed. A stereo calibration consists of determining the (fixed) displacement of the right camera reference frame with respect to the left camera. Stereo triangulation makes use of the fact that each pixel location on an image defines a ray, hence determining a point in 3D becomes the geometric problem of finding the closest point between two rays (ideally, the two rays would intersect).

The process of actually determining which points correspond between the left and right images is done "by hand." The corresponding spikes from the left and right images are shown in figure 3.2, where same numbers correspond to the same spike. The ability to recognize the same object from different perspectives is known as the "correspondence problem" and is an unsolved problem in computer science. For accurate correspondence, it is necessary to have a well-defined point in the object which is photographed, visible, and identifiable in both camera views. For the purposes of this experiment, that point is the tip of a spike. Accuracies of various calibration routines, when an object of known geometry is compared to the geometry measured using a stereo-triangulation method, have been reported to be one part in a thousand [15].

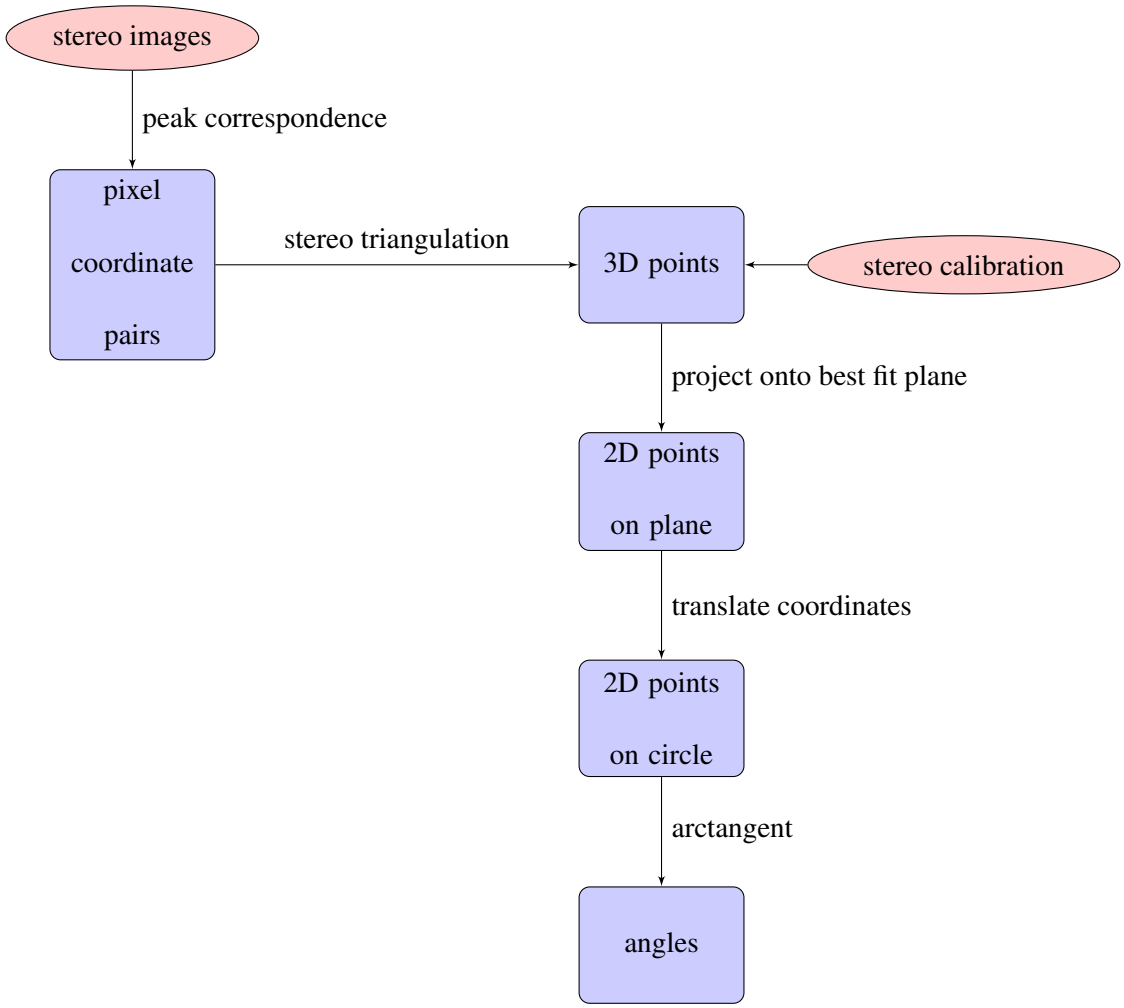

Figure 3.3: Data analysis flowchart: a set of stereo pixel coordinate pairs are reduced to a set of angles.

3.2.2 Data analysis procedure

The data analysis procedure is summarized in the flow chart in figure 3.3. We now give a detailed description of the analysis procedure which begins with a pair of images and ends with a set of angles $\mathbf{\Theta}$.

The algorithm requires two inputs: two stereo images and a stereo calibration. The first step is to identify the corresponding spikes in each of the left and right images; the result for a pair

of images is shown in figure 3.2.

The two pixel coordinate pairs, (x_l, y_l) and (x_r, y_r), are the input for the stereo triangulation function. Stereo triangulation gives the position of the point defined by the pair of pixel coordinates in the frame of the left camera: (X_l, Y_l, Z_l). The stereo triangulation step is implemented using a function provided by the Calibration Toolbox [2]. The details of stereo triangulation, including a derivation, may be found in [1].

With the 3D data now available, the next three steps reduce these data to a set of 1D angles. Since (X_l, Y_l, Z_l) are in the frame of the left camera, whose position relative to the location of the rim is arbitrary, the result of even an ideal rim is a set of points lying on a circle which has been rotated and translated. Instead of directly fitting a general rotated and translated circle in 3D which is nonlinear, we break up the task into two linear steps: fitting a plane, and then fitting a circle in a plane.

A plane is fitted to the data in a least-squares sense. The result is a plane defined by a normal z' vector. To rotate the current reference frame defined by normal z, we make use of Rodrigues' rotation formula [16]. To create a rotation vector we first need a direction in which to rotate. The direction of rotation desired is from z to z', which gives a rotation vector according to the right hand rule: $v_{rot} = z \times z'$. The magnitude of the desired rotation may be obtained by considering the dot product between z and z', which gives the angle of rotation $\theta_{rot} = \arccos(z \cdot z')$. The result of implementing Rodrigues' formula is a rotation matrix R. The rotation then is $(X, Y, Z)^T = R\,(X_l, Y_l, Z_l)^T$ and the projection onto the plane is obtained by setting $Z = 0$.

The resulting (X, Y) fit a circle which may be displaced from the origin. A further step is required to fit a circle, again in a least-squares sense. The fitted circle has a center (X_c, Y_c). By

taking $(X, Y) \rightarrow (X - X_c, Y - Y_c)$, the center of the circle coincides with the origin of the axes.

Once the data are centered, the arctangent function may be used to calculate the angle of a given point on a circle from the X-axis. To keep the quadrant information, the special function atan_2 in Matlab is used. The data points do not lie exactly on the fitted circle, therefore each angle extracted represents the point closest to the circle.

3.2.3 Experimental issues

The experimental setup, as described, involves a delicate balancing of the two groups systems. In particular, several points are worth discussing in detail. First we will discuss the high-speed camera and adequate lighting.

The high-speed cameras have a fixed buffer size and maximum amount of data the cameras can process per unit time. This translates to a balancing of frame rate and pixel resolution. To capture the dynamics of the drop splash, a frame rate of 1600 frames per second is required. This translates to a resolution of 768x768 pixels, or about half the full resolution. At this frame rate, typical lighting leaves the images underexposed. A high intensity halogen bulb of 600W are sufficiently bright (luminous), but also generate excessive heat. The film temperature was observed to rise a degree Celsius in a matter of seconds! Fortunately, there exist comparably bright LED bulbs which generate as much light as a traditional 600W bulb but with the heating of an 18W bulb.

The typical mechanism, by which the depth of field is increased, is to increase the f-number, thereby decreasing the aperture and letting in less light. Given the difficulty obtaining sufficiently exposed frames, a small aperture is not always possible. The result is balancing of f-number and frame exposure.

The last experimental concern is the liquid properties. Water is a well-characterized fluid,

but is quite transparent in the optical wavelengths. As a result, water is very difficult to visualize because it offers little contrast. Milk was used because it is opaque and offers much better contrast, as well as due to its use in the classical experiments.

3.2.4 Sources of error

Experimental errors, or uncertainties, can be divided into two categories associated with generating and recording the drop splash. The first type of errors are incurred while running the experiment and are due to physical imprecisions. Errors of this type might be responsible for the generation of an irregular crown when a regular crown is expected. The second type of error is incurred during the data analysis process, after the experiment is over.

Errors from physical setup

Among various measured quantities, the film thickness is perhaps the most uncertain. In theory, a gravimetric measurement is quite precise because it depends on measurements of length and mass – each of which can be made very accurately. In practice, working with milk rather than water introduces uncertainties due the added uncertainty of the density. A second, unquantified uncertainty is the flatness of the film because only a leveling bubble was used. For the calculation of film thickness we assume that the film thickness is uniform over the entire wetted surface. These two unknown factors contribute to a film thickness measurement that is more uncertain than one might naively calculate from the measurements and is $O(0.1mm)$. Given that the film thickness is less than $1mm$, the relative uncertainty is perhaps as large as 10%.

The droplet has two primary characteristics its diameter and velocity at impact. The velocity at impact is entirely due to gravitational acceleration (neglecting drag). Thus an accurate

measurement of the drop height gives a satisfactory calculation of impact velocity in the vertical direction. The droplet ideally has only vertical velocity, but some horizontal velocity can be induced if the syringe is not vertically aligned. The vertical alignment of the syringe is performed "by eye" and thus is relatively uncertain. The droplet diameter, for a given fixed configuration, may be measured gravimetrically and averaged over a number of droplets. The droplet mass is observed to be uniform over a large number of drops, hence averaging is justified. Therefore, the relative uncertainty in the droplet diameter is about 1%.

Errors from data reduction and analysis

The first source of error is incurred while determining the pixel coordinates of corresponding spikes. Ultimately, this error is due to how well the same spike location can be identified in each image. Part of the difficulty stems from the problem of definition: there are cases where the "tip of the spike" is not well-defined, i.e. it may be very rounded or flat. The focus and depth of field affect how visible the spikes are in each image. Finally the number of pixels, or the resolution, is a determining factor of the accuracy of the data. These three factors: spike definition, focus, and resolution contribute to an uncertainty radius of O(5 pixels) centered on each identified spike location in an image. Carrying the error analysis though the data reduction process was beyond the scope of this project but on the basis of many experiments, the uncertainty in the measurement of each angle is probably $O(10^\circ)$.

3.3 Examples of data analysis

We demonstrate the experimental methodology and theoretical basis with two sets of data from two drop splash experiments. While the theoretical treatment is rigorous for the qualified theoretical cases outlined above, treating the complexities inherent in experimental data requires some discussion and judgment.

3.3.1 A regular pattern with scatter

Analyzing the stereo images in figure 3.2, the results of the data analysis procedure and pattern identification are shown in figure 3.4. The physical parameters are the drop height $H = 28cm$, film thickness $h = 0.89mm$, and the droplet diameter $d = 4.4mm$ for Knudsen 2% milk at room temperature. The dimensionless variables are $We_{\text{drop}} = 605$ and an inertia ratio $\alpha = d/h = 5$.

The result of stereo triangulation, in the frame of the left camera, is displayed in figure 3.4(a). After changing coordinates, we see in figure 3.4(b) that the variance in the z-direction is much less than that in the $x - y$ directions. This fact confirms what we can see from images, that the tips of the spikes of the rim are nearly coplanar.

Before calculating angles, we check that the data in figure 3.4(c) fit a circle well. With the exception of a projection onto a plane, the data are not altered in the process of the rotation and translation (which may be viewed as coordinate transformations); it is fortunate that the data *happen* to fit a circle to a good approximation.

The complex order amplitudes are plotted in figure 3.4(d) and interpreted like a power spectrum of the Fourier transform. We note that prominent values correspond to orders $m = 21, 22, 23$ and the lack of a clear single dominating order. Therefore the order parameter plot is

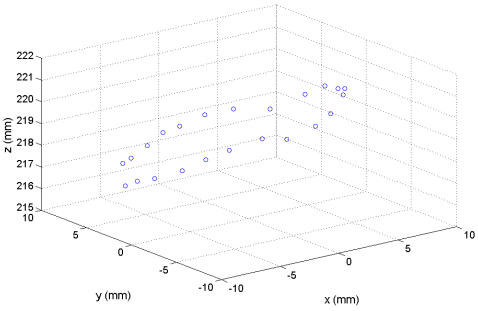

(a) Result of stereo triangulation.

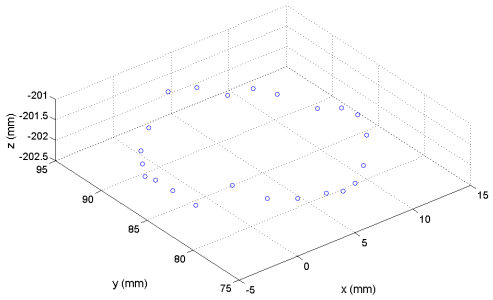

(b) After rotation.

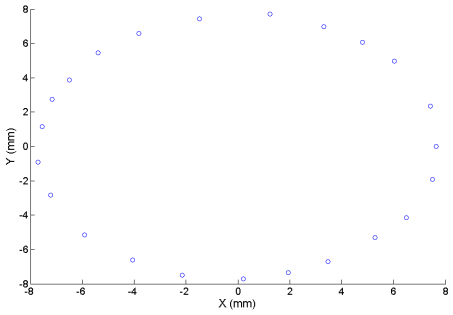

(c) Data projected onto a plane.

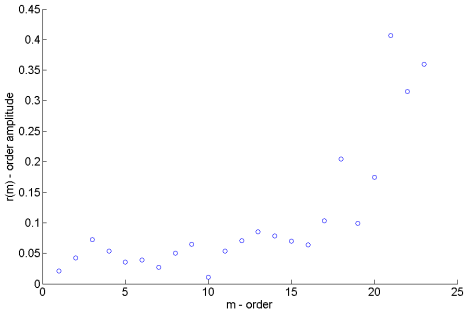

(d) Complex order amplitudes.

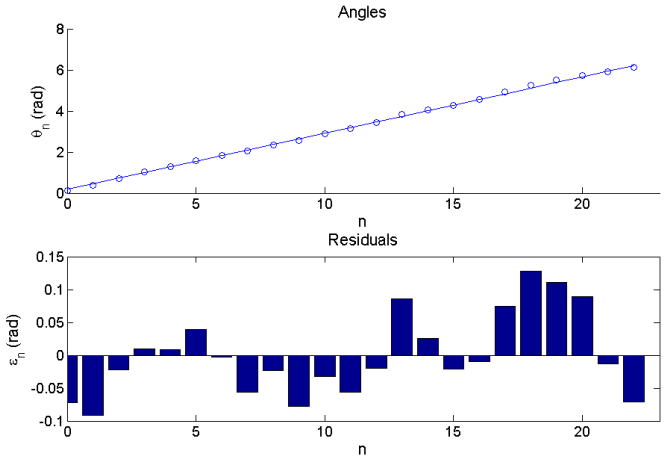

(e) Extracted angles and residuals.

Figure 3.4: Example of data reduction and analysis: (a) results of triangulation in the reference frame of the left camera, (b) first coordinate transform, (c) second coordinate transform, (e) the resulting fit with residuals, and (d) the plot of complex order amplitudes for the crown in figure 3.2, $We_{\text{drop}} = 605$, $H = 28cm$, $\alpha = 5$, Knudsen 2% milk.

inconclusive, but we may interpret it to indicate the possible presence of a one single-wavenumber pattern (perhaps $k = 23$) with considerable scatter.

For figure 3.4(e), we assume the data are composed of a complete single-wavenumber pattern with scatter. Therefore the wavenumber is the number of points, $k = 23$, and we calculate the scatter δ. To quantify the quality of the fit we consider the scatter ratio: $\delta/\lambda = 0.94$. A scatter ratio so close to unity indicates that the fit is "correct" in the sense that it conforms with the definition presented for a single-wavenumber with scatter – however, the fit is far from ideal.

On physical grounds we may reinforce the expectation that data are a single-wavenumber pattern. First, from the earliest stages in the drop splash recording it is qualitatively clear that the spikes are uniformly spaced. To be able to confidently correspond the tips of spikes in the rim – without which no measurements can be made – it was necessary to wait for the rim to more fully develop. The presence of surface tension is observed to scatter the ideal single-wavenumber pattern as the rim develops into the later stages. Along with the fact that all the spikes are observed to be accounted for, we expect a complete single-wavenumber pattern with scatter.

3.3.2 An irregular rim

Given the difficulties introduced by a regular rim above, one would expect ambiguities for the apparently irregular rim in figure 3.5(a). This pattern was generated using same conditions as for the regular case but with a *smaller* droplet height, giving $We_{\text{drop}} = 345$. One might expect regular patterns for lower impact energies and irregular patterns for higher impact energies; however, this simple explanation is not observed in experiments.

In figure 3.5(b), we see that interpreting the data as a complete single-wavenumber pattern with scatter is inappropriate. Furthermore, the complex order parameter amplitudes in figure 3.5(c)

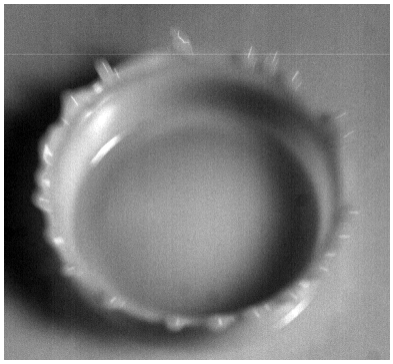

(a) Right image.

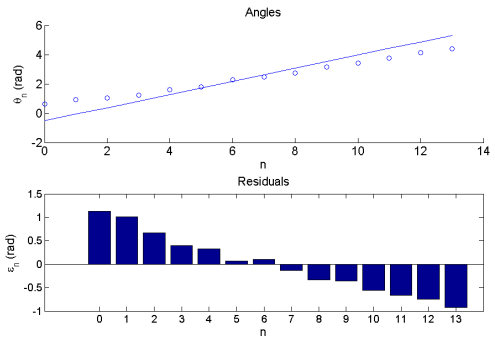

(b) Attempt to fit a complete regular pattern.

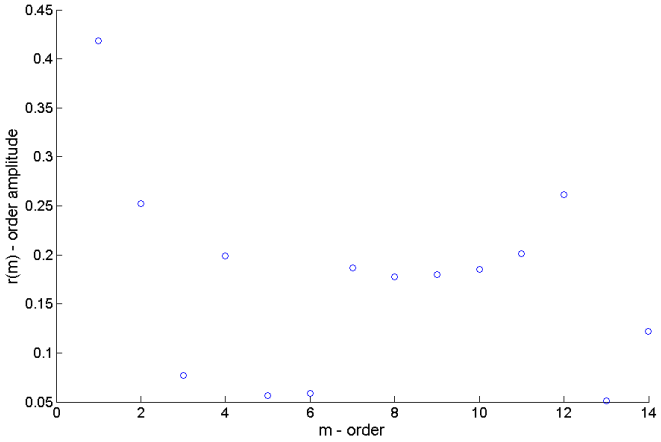

(c) Complex order parameter amplitudes.

Figure 3.5: The case of an irregular rim: (a) the right image of the rim, (b) attempt to fit a single-wavenumber pattern, (c) the plot of complex order amplitudes for $We_{\text{drop}} = 345$, $\alpha = 5$, Knudsen 2% milk.

do not indicate any dominate wavenumber(s). While the data may correspond to a regular pattern for *some* scatter, it appears irregular at this stage. Due to possible presence of overlaps, missing points, and large scatter, one cannot conclusively say that the pattern cannot be identified as regular for *some* decomposition.

Chapter 4

Conclusions

A novel experimental method has been developed in order to analyze the rim resulting from a drop splash. In particular, it is possible to use stereo triangulation and a process of data reduction to measure the angular position of each spike in the rim. Analysis of the drop splash crown has motivated the development of "pattern identification theory." This theoretical framework is applicable to a broader range of physical problems with O(2) symmetry.

This thesis lays out a theoretical framework for wavenumber spaces. First, we considered the case of ideal patterns without scatter. Scatter was then introduced as a generalization without considerable difficulty. Some key insights into the nature of wavenumber spaces were required to deal with the case of patterns with overlaps. The case of incomplete patterns remains a challenge, though a step has been taken towards better understanding when they are well-defined.

Much work remains to be done. Analyzing the errors associated with stereo triangulation and various coordinate transformations was beyond the scope of this project. To rigorously conclude if a pattern is regular requires a better understanding of the experimental uncertainties

involved. Towards that end, more case studies of a single wavenumber pattern with less scatter are desirable because they would first verify the analysis, and second enable the statistical determination of uncertainties. Lastly, the most general case of incomplete patterns with scatter and possible overlaps remains to be tackled. This general case may be most useful when analyzing experimental data.

Bibliography

[1] Jean-Yves Bouguet. *Visual methods for three-dimensional modeling*. PhD thesis, Caltech, 1999.

[2] Jean-Yves Bouguet. Camera calibration toolbox for matlab. `http://www.vision.caltech.edu/bouguetj/calib_doc/index.html`, June 2008.

[3] John Buck. Synchronous rhythmic flashing of fireflies. II. *Quarterly Review of Biology*, 63:265–289, 1988.

[4] T. A. Clark and J. G. Fryer. The development of camera calibration methods and models. *Photogrammetric Record*, 16(91):51–66, 1998.

[5] R. D. Deegan, P. Brunet, and J. Eggers. Rayleigh-Plateau instability causes the crown splash. *ArXiv e-prints*, June 2008.

[6] Harold Edgerton. Exploring photography: Photographers: Harold edgerton. `http://www.vam.ac.uk/vastatic/microsites/photography/photographer.php?photographerid=ph019&row=4`, 2002.

[7] Jose Maria Fullana and Stephane Zaleski. Stability of a growing end rim in a liquid sheet of uniform thickness. *Physics of Fluids*, 11(5):952–954, 1999.

[8] Janne Heikkila and Olli Silven. A four-step camera calibration procedure with implicit image correction. *Computer Vision and Pattern Recognition, IEEE Computer Society Conference on*, 0:1106, 1997.

[9] Rouslan Krechetnikov. Rayleigh-Taylor and Richtmyer-Meshkov instabilities of flat and curved interfaces. *Journal of Fluid Mechanics*, 625:387–410, 2009.

[10] Rouslan Krechetnikov. Stability of liquid sheet edges. *Physics of Fluids*, 2010. to appear.

[11] Rouslan Krechetnikov and George M. Homsy. Crown-forming instability phenomena in the drop splash problem. *Journal of Colloid and Interface Science*, 331(1):555–559, 2008.

[12] K. V. Mardia. *Directional statistics*. Wiley, Chichester, New York, 2000.

[13] Steven H. Strogatz. From Kuramoto to Crawford: exploring the onset of synchronization in populations of coupled oscillators. *Physica D*, 120:1–20, 2000.

[14] John R. Taylor. *An Introduction to Error Analysis*. University Science Books, Sausalito, 2 edition, 1997.

[15] Roger Y. Tsai. A versatile camera calibration technique for high-accuracy 3d machine vision metrology using off-the-shelf tv cameras and lenses. *Journal of Robotics and Automation*, RA-3(4):323–344, 1987.

[16] Wikipedia. Rodrigues' rotation formula. `http://en.wikipedia.org/wiki/Rodrigues'_rotation_formula`, July 2010.

[17] Zhengyou Zhang. Flexible camera calibration by viewing a plane from unknown orientations. In *ICCV*, pages 666–673, 1999.